IEEE Photonics Journal
An IEEE Photonics Society Publication

Open Access

Ultra-Broadband Polarization Beam Splitter Based on Cascaded Mach-Zehnder Interferometers Assisted by Effectively Anisotropic Structures

Volume 13, Number 1, February 2021

Zongxing Lin
Kaixuan Chen
Qiangsheng Huang
Sailing He, *Fellow, IEEE*

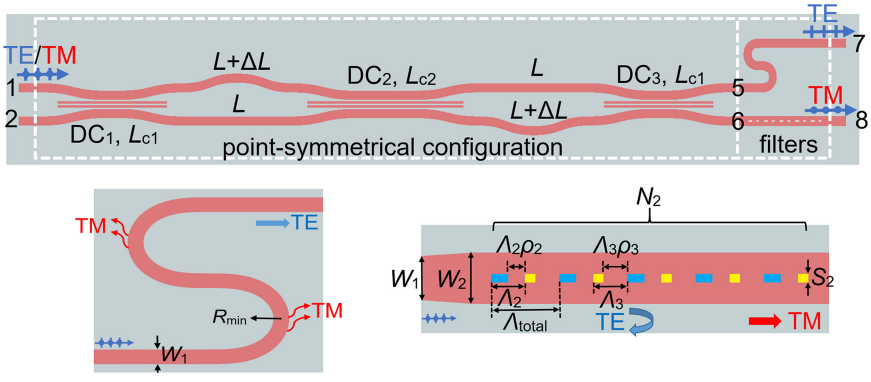

DOI: 10.1109/JPHOT.2021.3050114

Ultra-Broadband Polarization Beam Splitter Based on Cascaded Mach-Zehnder Interferometers Assisted by Effectively Anisotropic Structures

Zongxing Lin,[1,2] **Kaixuan Chen**,[1,3] **Qiangsheng Huang,**[1] **and Sailing He**,[1,2,3] ***Fellow, IEEE***

[1]Center for Optical and Electromagnetic Research, National Engineering Research Center for Optical Instruments, Zhejiang University, Zijingang Campus, Hangzhou 310058, China
[2]Ningbo Research Institute, Zhejiang University, Ningbo 315100, China
[3]Centre for Optical and Electromagnetic Research, South China Academy of Advanced Optoelectronics, South China Normal University, Guangzhou 510006, China

DOI:10.1109/JPHOT.2021.3050114
This work is licensed under a Creative Commons Attribution 4.0 License. For more information, see https://creativecommons.org/licenses/by/4.0/

Manuscript received November 13, 2020; revised December 30, 2020; accepted January 5, 2021. Date of publication January 8, 2021; date of current version January 25, 2021. This work was supported in part by the National Key Research and Development Program of China under Grant 2018YFB2200200, in part by the National Natural Science Foundation of China under Grant 11621101, and in part by Ningbo Science and Technology Project under Grant 2018B10093. Corresponding author: Sailing He (e-mail: sailing@kth.se).

Abstract: An ultra-broadband polarization beam splitter (PBS) consisting of cascaded Mach-Zehnder interferometers (MZIs) is proposed on 220 nm-thick silicon-on-insulator (SOI) platform. The configuration of the cascaded MZIs has a point symmetry in order to broaden the bandwidth of the cross-coupling for the TM polarization. The sub-wavelength grating (SWG) structures act as effectively anisotropic cladding to enhance the separation of the two fundamental polarizations. Two filters with cascaded bends and a Bragg reflection structure at the two outputs, respectively, are used to further improve the extinction ratio (ER). The proposed PBS has a remarkable performance with ER $>$ 20 dB over a record broad bandwidth of 310 nm (IL $<$ 0.5 dB) or 350nm (IL $<$ 1 dB) for both TE and TM polarization inputs.

Index Terms: Polarization beam splitter (PBS), sub-wavelength grating (SWG), anisotropic metamaterial, ultra-broadband.

1. Introduction

Over the last decade, silicon photonics based on silicon-on-insulator (SOI) has attracted more and more interests due to the advantages of high index contrast, compact footprint and compatibility to the complementary metal oxide semiconductor (CMOS). However, the high index contrast results in waveguide birefringence and makes the silicon nanophotonic devices polarization dependent. In order to solve this problem, polarization management is required. One of the most important devices for polarization management is polarization beam splitter (PBS), which can separate the two orthogonal polarizations. Various PBSs on silicon chip have been reported by using different structures, such as Mach-Zehnder interferometers (MZIs) [1], [2], multi-mode interference (MMI) couplers [3]–[5], and directional couplers (DCs) [6]–[12]. Among these structures, DC is often used

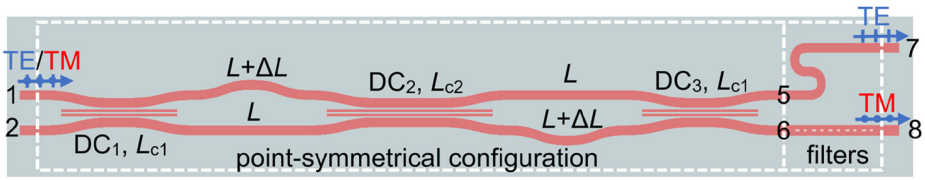

Fig. 1. Schematic configuration of the proposed PBS.

due to its simple design and good performance. However, DC is wavelength dependent and the bandwidth of a PBS based on such a structure is often limited to 100 nm.

Recently, the sub-wavelength grating (SWG) structure has attracted much attention due to its robust freedom for index and dispersion engineering. The SWG structure is formed by different index materials alternating periodically and the grating period is much small than the wavelength. For light propagating in the SWG structure, according to Rytov's formulas, the equivalent refractive indices for the electric field polarizations parallel and perpendicular to the periodic interfaces are different. Therefore, the SWG structure can be treated as equivalent homogeneous material and we can control the dispersion relation of the mode in the SWG waveguide by adjusting its period and duty cycle, which can be used to improve the device performance greatly [13]–[16]. A PBS formed by SWG structures, working as two isolated waveguides for the TE polarization and MMI for the TM polarization, has achieved ER $>$20 dB and IL $<$1 dB over a bandwidth of 200nm experimentally [17]. In [18], a PBS using cascaded adiabatic dual-core tapers assisted by SWG structure gives ER $>$ 20 dB over a bandwidth of 240 nm experimentally.

In our previous work, by taking advantage of polarization-dependent evanescent wave control via the SWG as effectively anisotropic structures in the cascaded DCs, we have designed theoretically a PBS with ER $>$ 20 dB and IL $<$ 0.4 dB over a bandwidth of 250 nm [19]. In this paper, by using the cascaded MZIs assisted by SWG structures and two filters at the two outputs, we further improve the bandwidth and reduce the footprint of the PBS than before.

2. Design and Analysis

Fig. 1 shows the schematic configuration of the proposed PBS, which consists of cascaded MZIs and two filters shown in the first and second white dashed frames, respectively. It is on a 220-nm-thick SOI platform with silicon dioxide upper-cladding. When light inputs to port 1, the TE polarization will go through three DCs along its original waveguide and output from port 7 with negligible coupling, while the TM polarization will cause some interference in MZIs and output from port 8 finally. The configuration of the cascaded MZIs has the point symmetry, which guarantees the broadband output from port 8 for the TM polarization. The bend structure at port 7 and the Bragg reflection structure at port 8 would filter out the remaining TM and TE powers, respectively.

2.1 DC Used in the Proposed PBS

Fig. 2(a) shows the configuration of the single DC used in the PBS. This DC consists of a normal DC and SWG structure in the coupling region. By inserting the SWG structure in the coupling region of a normal DC and selecting the period Λ_1, the duty cycle of silicon ρ_1 and the total number of periods N_1 of the SWG structure, the decay rate of the TE polarization or the TM polarization can be suppressed or enhanced [19]–[21]. Therefore, when light travels in the coupling region in a DC, there is almost no coupling for the TE polarization but strong coupling for the TM polarization. Due to the coupling existing in S-bend waveguides, the length of the SWG structure L_c+2L_t is larger than the length of the straight coupling region L_c. Fig. 2(b) shows the cross section of the straight coupling region in DC.

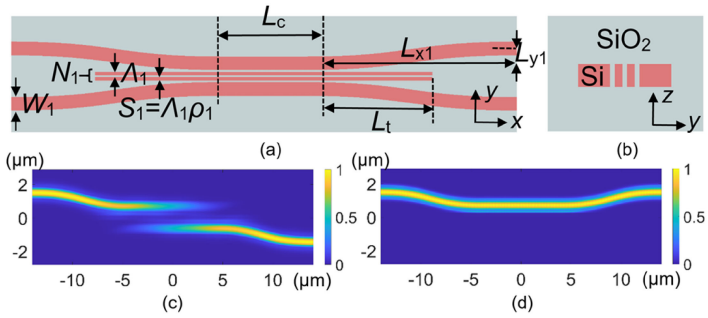

Fig. 2. (a) Schematic configuration of the DC used in the proposed PBS. (b) The cross section of the straight coupling region in DC. (c) Simulated light propagation of the TM polarization in DC with $L_c = 8\ \mu$m at wavelength $\lambda = 1.55\ \mu$m. (d) Simulated light propagation of the TE polarization in DC with $L_c = 8\ \mu$m at wavelength $\lambda = 1.55\ \mu$m.

TABLE 1
List of the Design Parameters for the Proposed DC

W_1	L_t	L_{x1}	L_{y1}	Λ_1	ρ_1	S_1	N_1
0.55 μm	8 μm	10 μm	0.6 μm	210 nm	130/210	130 nm	2

For the proposed DC, the width of the coupled waveguides is set at $W_1 = 0.55\ \mu$m and the S-bend waveguides are based on the second order Bezier curve (the corresponding four points are (0,0), (L_{x1}/2,0), (L_{x1}/2, L_{y1}), (L_{x1}, L_{y1}) or (0, L_{y1}), (L_{x1}/2, L_{y1}), (L_{x1}/2, 0), (L_{x1}, 0)) with $L_{x1} = 10\ \mu$m, $L_{y1} = 0.6\ \mu$m to reduce the bending loss. The parameters of the SWG structure should be optimized to enhance the coupling for the TM polarization and make the coupling of the TE polarization negligible in the whole cascaded structure. The optimized parameters are $\Lambda_1 = 210$ nm, $\rho_1 = 130/210$, $N_1 = 2$ and $L_t = 8\ \mu$m so that the gap of the SWG structure is 80 nm and the width of the SWG structure waveguide is $S_1 = 130$ nm, which also ensures that the SWG structure works in deep-subwavelength region and can be fabricated with existing nanometer-scale fabrication techniques. Fig. 2(c) and 2(d) show the simulated light propagation for the TE and TM polarizations in the proposed DC with $L_c = 8\ \mu$m at wavelength $\lambda = 1.55\ \mu$m, respectively. One can see that the TE polarization goes through the DC with negligible coupling while the TM polarization totally couples across the DC. Table 1 summarizes the design parameters for the proposed DC.

2.2 Point Symmetrical Configuration Constructed by Cascaded MZIs

An effective way to reduce the wavelength dependency of DC is to use MZI configuration, which consists of two DCs and two phase delay arms with a small difference. A broadband coupling in the MZI configuration can be achieved due to the phase compensation in different wavelengths [22]–[24]. Consisting of two cascaded MZIs, the point symmetrical configuration is shown in the first white dashed frame in Fig. 1 and is described in detail in Fig. 3(a). The three DCs have the same parameters as described in Part 2.1 except the length of the straight coupling region (the length of the straight coupling region of three DCs are L_{c1}, L_{c2}, and L_{c1} respectively). The DC_1 and one half of DC_2 with a small path difference ΔL in the two arms between them form the first MZI, and the other half of DC_2 and DC_3 with a small path difference -ΔL in the two arms between them form the second MZI, as shown in the first and second yellow dashed frames in Fig. 3(a) respectively. If the TM polarization is split by 50:50 by the first MZI, then it would be combined by the second MZI and outputs from port 6 [25]. As for the TE polarization, the coupling in DCs is so weak that the TE polarization would go through the three DCs and output from port 5. Finally, the

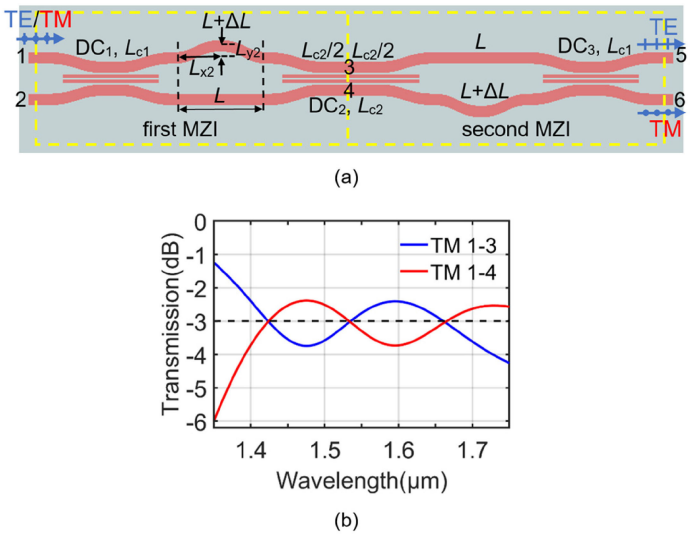

Fig. 3. (a) Detailed description of the point symmetrical configuration. (b) Transmission of the first MZI for the TM polarization.

two fundamental polarizations are separated and the bandwidth mostly depends on the bandwidth of the MZI splitting 50:50 for the TM polarization.

For this cascaded structure, it is convenient to use transfer matrix to calculate [19]. For a single DC with straight coupling length L_c in Fig. 2(a), its transfer matrix can be written as

$$A_{L_c+L_0} = \begin{bmatrix} \cos\theta & j\sin\theta \\ j\sin\theta & \cos\theta \end{bmatrix} = \begin{bmatrix} \cos\left(k\left(L_c+L_0\right)\right) & j\sin\left(k\left(L_c+L_0\right)\right) \\ j\sin\left(k\left(L_c+L_0\right)\right) & \cos\left(k\left(L_c+L_0\right)\right) \end{bmatrix} \tag{1}$$

where k is the coupling constant in the straight coupling region and L_0 is the equivalent coupling length introduced by S-bend waveguides.

According to the supermode theory, the coupling constant in the straight coupling region can be expressed as

$$k = \frac{k_0}{2}\left(n_{\text{eff,even}} - n_{\text{eff,odd}}\right) \tag{2}$$

where k_0 is the wave vector in free space and $n_{\text{eff,even}}$, $n_{\text{eff,odd}}$ are the effective indices of even and odd modes in straight coupling region, respectively.

For two arms with a small path difference ΔL between two DCs, the transfer matrix can be written as

$$B_{\Delta L} = \begin{bmatrix} e^{j\Delta\varphi} & 0 \\ 0 & 1 \end{bmatrix} = \begin{bmatrix} e^{j\beta\Delta L} & 0 \\ 0 & 1 \end{bmatrix} = \begin{bmatrix} e^{jn_{\text{eff}}k_0\Delta L} & 0 \\ 0 & 1 \end{bmatrix} \tag{3}$$

where $\Delta\varphi = \beta\Delta L$ is the phase shift introduced by ΔL, β and n_{eff} are the propagation constant and effective index of an uncoupled waveguide mode, respectively.

Thus, the transmission of the first MZI and point symmetrical configuration can be expressed as

$$\begin{bmatrix} E_3 \\ E_4 \end{bmatrix} = A_{(L_{c2}+L_0)/2}\, B_{\Delta L} A_{L_{c1}+L_0} \begin{bmatrix} E_1 \\ E_2 \end{bmatrix} \tag{4}$$

$$\begin{bmatrix} E_5 \\ E_6 \end{bmatrix} = A_{L_{c1}+L_0} B_{-\Delta L} A_{L_{c2}+L_0}\, B_{\Delta L} A_{L_{c1}+L_0} \begin{bmatrix} E_1 \\ E_2 \end{bmatrix} \tag{5}$$

where $A_{L_{c1}+L_0}$ is the transfer matrix of DC_1 and DC_3, $A_{L_{c2}+L_0}$ is the transfer matrix of DC_2, $A_{(L_{c2}+L_0)/2}$ is the transfer matrix for half of DC_2, E_1 and E_2 are the input amplitudes in ports 1 and 2, and E_3,

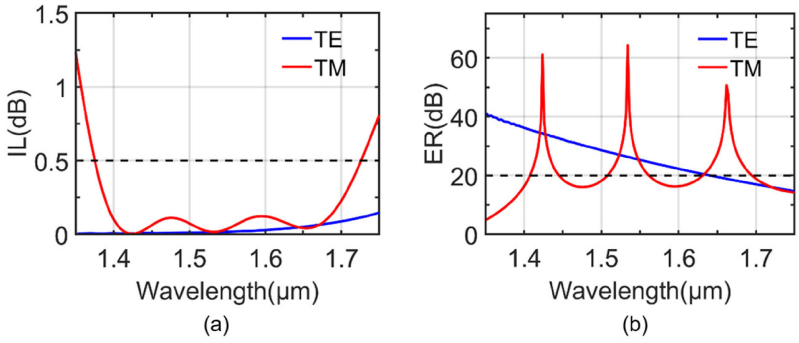

Fig. 4. Calculated IL and ER of the point symmetrical configuration. (a) IL for the TE and TM polarizations. (b) ER for the TE and TM polarizations.

E_4, E_5, E_6 are the output amplitudes from ports 3, 4, 5, 6. When light inputs at port 1, we have $E_1 = 1$ and $E_2 = 0$. Using Eqs. (4) and (5), we can obtain the output power portions from port i ($i = 3$, 4, 5, 6) by $I_i = |E_i|^2$.

For the point symmetrical configuration, the uncertain parameters are L_{c1}, L_{c2} and ΔL, and we must optimize them with Eq. (4) or (5) to make sure that the MZI can split the TM polarization by 50:50 in an ultra-broadband. The calculation process is summarized as follows: Firstly, we simulate a single DC with $L_c = 0$ by Lumerical FDTD solutions to get its transmission and loss. Secondly, we calculate the effective indices $n_{\text{eff,even}}$, $n_{\text{eff,odd}}$ and n_{eff} by Lumerical MODE Solutions. According to the supermode theory, we can obtain L_0 for DC. Finally, the outputs can be calculated through Eq. (4) or (5) and the parameters are optimized to $L_{c1} = 0.1$ μm, $L_{c2} = 18.1$ μm and $\Delta L = 0.58$ μm. Fig. 3(b) shows the transmission of the first MZI at the optimized parameters for the TM polarization. One can see that in an ultra-broadband bandwidth from 1.4 μm to 1.7 μm, the outputs from ports 3 and 4 vary between -3$\pm$1dB.

We then calculate the IL and ER for TE and TM polarizations based on the optimized parameters. Here, the IL and ER are defined as

$$\begin{aligned} \text{IL}_{\text{TE}} &= -10\log_{10} I_5, \ \text{ER}_{\text{TE}} = -10\log_{10}\left(\frac{I_6}{I_5}\right) \\ \text{IL}_{\text{TM}} &= -10\log_{10} I_6, \ \text{ER}_{\text{TM}} = -10\log_{10}\left(\frac{I_5}{I_6}\right) \end{aligned} \tag{6}$$

Fig. 4(a) and 4(b) show the calculated IL and ER of the point symmetrical configuration for the TE and TM polarizations. For the TE polarization, it has IL $<$ 0.25 dB over a bandwidth of 400 nm and ER $>$ 20 dB over a bandwidth of 280 nm. The ER deteriorates at longer wavelength due to the stronger coupling for long wavelength in DCs. For the TM polarization, we have achieved IL $<$ 0.5 dB over 350 nm but the ER is not good in some bands because splitting ratio in the first MZI is not exactly 50:50 in the whole ultra-broad bandwidth.

2.3. Improvement With Filters

In order to achieve better ERs, we introduce some simple filters at the two outputs, as shown by the second white dashed frame in Fig. 1. The detailed description is shown in Fig. 5(a) and 5(b).

When the waveguide cross section is 550 nm $\times$ 220 nm, the TM polarization has a larger bending loss than the TE polarization. Therefore, two cascaded 180° bends based on four 90° Euler curves are used to filter the remaining power of the TM polarization from port 5, as shown in Fig. 5(a). Bends based on Euler curves have varying radium of curvature, which can reduce the generation of high-order modes compared to traditional bends [26], [27]. Here, we set $R_{\min} = 0.72$ μm to make sure that the loss of these bends is large for the TM polarization but small for the TE polarization.

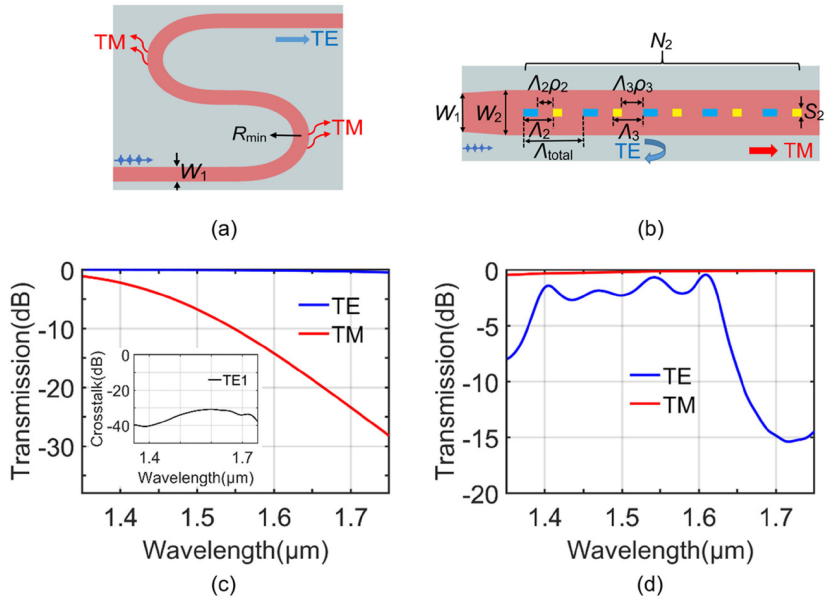

Fig. 5. (a) Two cascaded 180° bends used to improve the ER for the TM polarization. (b) Interleaved SWGs used to improve the ER for the TE polarization. (c) Transmission of the two cascaded 180° bends. (d) Transmission of the interleaved SWGs. Inset in (c) is the crosstalk of the first-order TE polarization (TE1).

The transmission of the two cascaded 180° bends is shown in Fig. 5(c). One can see that these bends have small loss for the TE polarization but very high loss for the TM polarization in an ultra-broad bandwidth. Inset in Fig. 5(c) is the crosstalk of the first-order TE polarization (TE1), which is less than -30 dB. This means that the crosstalk of high-order modes in these two cascaded 180° bends is negligible and almost has no impact on the performance.

Two interleaved SWGs are introduced in the strip waveguide to filter the remaining power of the TE polarization from port 6, as shown by blue and yellow squares in Fig. 5(b). One should note that the blue and yellow squares are full etched squares filling with silicon dioxide upper-cladding and different colors are used just to describe the shapes and distinguish them. S_2 is the width of the SWGs, W_2 is the width of strip waveguide, ρ_i, Λ_i are the duty cycle of silicon and period of the i-th ($i = 2, 3$) SWGs and the total period is $\Lambda_{\text{total}} = \Lambda_2 + \Lambda_3$. By optimizing these parameters, this structure can support Bloch mode for the TM polarization only [28]. Hence, the TM polarization can travel along the strip waveguide with rather low loss while the TE polarization would be completely reflected by the embedded SWG structure due to the Bragg reflection. As shown in Fig. 4(b), the ER for the TE polarization degrades as the wavelength increases. Therefore, we optimized the parameters to let the central wavelength for the reflected TE polarization light be located near 1.75 μm. The optimized parameters are $S_2 = 100$ nm, $W_2 = 0.6$ μm, $\rho_2 = 0.5$, $\rho_3 = 0.7$, $\Lambda_2 = \Lambda_3 = 400$ nm and the total number of periods is $N_2 = 5$. Since W_2 is a bit lager than W_1 of DC, a taper should be used to connect them. The transmission of the interleaved SWGs is shown in Fig. 5(d). One can see that the interleaved SWGs have very small loss for the TM polarization in an ultra-broad bandwidth but reflect the TE polarization strongly in 1.65-1.75 μm wavelength range. Table 2 summarizes the design parameters for the filters.

Due to the nonuniformity of filtering, L_{c1}, L_{c2} and ΔL should be optimized again to get the best results. The re-optimized parameters are $L_{c1} = 1.8$ μm, $L_{c2} = 22$ μm and $\Delta L = 0.55$ μm. Fig. 6(a) and 6(b) show the ILs and ERs of the proposed PBS for the TE and TM polarizations. One can see that the bandwidth of ERs $>$ 20dB for both TE and TM polarizations is 360 nm (1.39-1.75 μm), which is much better compared to the results of the point symmetrical configuration. The filters also

TABLE 2
List of the Design Parameters for the Filters

R_{min}	W_2	Λ_2	ρ_2	Λ_3	ρ_3	Λ_{total}	S_2	N_2
0.72 μm	0.6 μm	400 nm	0.5	400 nm	0.7	800 nm	100 nm	5

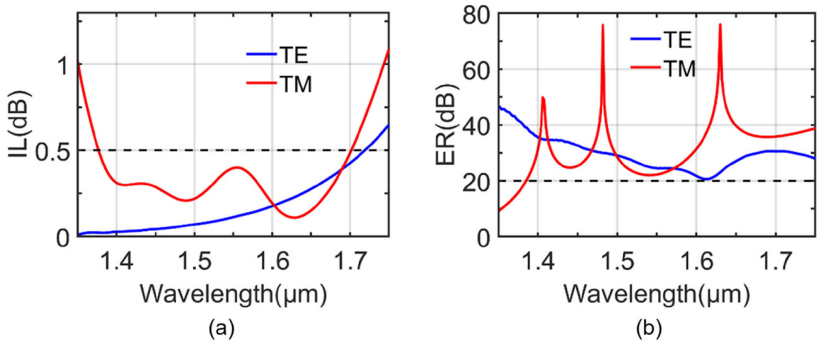

Fig. 6. Calculated IL and ER of the proposed PBS. (a) IL for the TE and TM polarizations. (b) ER for the TE and TM polarizations.

introduce some additional but acceptable loss. For both TE and TM polarizations, the bandwidth for IL $<$ 0.5 dB and ER $>$ 20 dB is over 310 nm (1.39-1.7 μm) and the bandwidth for IL $<$ 1 dB and ER $>$ 20 dB is over 350 nm (1.39-1.74 μm). To the best of our knowledge, these are the largest bandwidths that have ever been reported.

3. Tolerance Analysis

The fabrication tolerance of the proposed PBS is analyzed, as shown in Fig. 7 and 8.

In Fig. 7, we assume that all waveguide widths in the proposed PBS, including W_1, S_1, W_2 and S_2, have the same variation ΔW while the center-to-center distance of waveguides is fixed, which would also change ρ_1, ρ_2 and ρ_3. From Fig. 7(a) and 7(b), one can see that the IL and ER for the TE polarization vary only slightly when ΔW changes by $\pm$5 nm and $\pm$10 nm, which means that the TE polarization is insensitive to the change ΔW. This is because the TE polarization goes through the three DCs with negligible coupling. Compared to the TE polarization, the TM polarization is more sensitive to the change ΔW, as shown in Fig. 7(c) and 7(d), due to the change in the transmission of the MZI caused by ΔW. When ΔW changes by $\pm$5 nm and $\pm$10 nm, the bandwidth for IL $<$ 0.5 dB and ER $>$ 20 dB is over 250 nm and 210 nm, respectively, which still covers a broad bandwidth.

Since the main principle of the proposed PBS is based on the interference of the TM polarization and the MZI is very sensitive to the phase shift caused by the two arms, the influence of the width variation between the two arms in the MZI is also investigated. Here, we set $L = 60$ μm, $L_{x2} = 30$ μm and $L_{y2} = 3.42$ μm (the S-bend arm of $L+\Delta L$ is also based on the second order Bezier curve) so that $\Delta L = 0.55$ μm and the S-bend has negligible loss and negligible impact on effective index compared to straight waveguide. The width of straight arm (length is L) is kept W_1 and the S-bend arm (length is $L+\Delta L$) has a width of $W_1 \pm \Delta W_{\Delta L}$. Fig. 8(a) and 8(b) show the IL and ER for the TM polarization when $\Delta W_{\Delta L}$ is $\pm$1 nm and $\pm$2 nm in the MZIs in the proposed PBS. When $\Delta W_{\Delta L}$ is $+$1 nm and $+$2 nm, the IL and ER for the TM polarization become deteriorated near 1.45 μm. When $\Delta W_{\Delta L}$ is -1 nm and -2 nm, the IL and ER for the TM polarization is still excellent in an ultra-broaden band but the first two peaks of the ER curve in 1.35-1.55 μm wavelength range

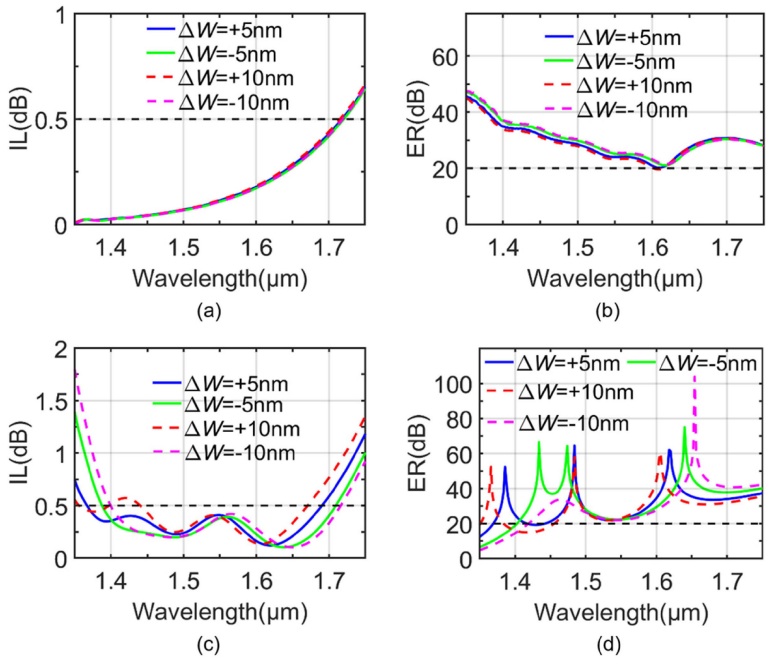

Fig. 7. Calculated ILs and ERs of the proposed PBS when ΔW changes by $\pm$5 nm and $\pm$10 nm. (a) IL for the TE polarization. (b) ER for the TE polarization. (c) IL for the TM polarization. (d) ER for the TM polarization.

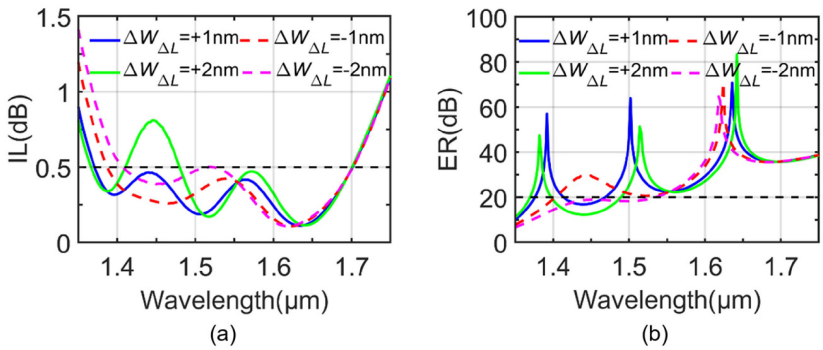

Fig. 8. Calculated ILs and ERs of the proposed PBS when $\Delta W_{\Delta L}$ changes by $\pm$1 nm and $\pm$2 nm. (a) IL for the TM polarization. (b) ER for the TM polarization.

disappear due to the increasing IL at these two peak wavelengths. A shorter L can reduce the influence of $\Delta W_{\Delta L}$ but would increase the bending loss in the S-bend arm and phase error.

4. Conclusion

In summary, we have proposed an ultra-broadband PBS consisting of cascaded MZIs on 220 nm thick silicon-on-insulator platform. The point symmetrical configuration of the cascaded MZIs can broaden the working bandwidth for the TM polarization. The SWG structures in DCs act as some effectively anisotropic cladding to enhance the separation of the two fundamental polarizations. At the two output ports of the point symmetrical configuration, two filters with two cascaded 180° bends and Bragg reflection structure have been used to improve the ER further. Calculated results

have shown that our proposed PBS has the remarkable performance with ER $>$ 20 dB over a record broad bandwidth of 310 nm (IL $<$ 0.5 dB) or 350nm (IL $<$ 1 dB) for both TE and TM polarization inputs. The fabrication tolerance analysis has shown that our proposed PBS can work well in the present of some fabrication errors.

References

[1] T. K. Liang and H. K. Tsang, "Integrated polarization beam splitter in high index contrast silicon-on-insulator waveguides," *IEEE Photon. Technol. Lett.*, vol. 17, no. 2, pp. 393–395, Feb. 2005.

[2] D. Dai, Z. Wang, J. Peters, and J. E. Bowers, "Compact polarization beam splitter using an asymmetrical mach–zehnder interferometer based on silicon-on-insulator waveguides," *IEEE Photon. Technol. Lett.*, vol. 24, no. 8, pp. 673–675, Apr. 15, 2012.

[3] J. M. Hong *et al.*, "Design and fabrication of a significantly shortened multimode interference coupler for polarization splitter application," *IEEE Photon. Technol. Lett.*, vol. 15, no. 1, pp. 72–74, Jan. 2003.

[4] X. Guan, H. Wu, Y. Shi, and D. Dai, "Extremely small polarization beam splitter based on a multimode interference coupler with a silicon hybrid plasmonic waveguide," *Opt. Lett.*, vol. 39**,** no. 2, pp. 259–262, 2014.

[5] Y. Huang, Z. Tu, H. Yi, Y. Li, X. Wang, and W. Hu, "Polarization beam splitter based on cascaded step-size multimode interference coupler," *Opt. Eng.*, vol. 52, no. 7, 2013, Art. no. 077103.

[6] H. Fukuda, K. Yamada, T. Tsuchizawa, T. Watanabe, H. Shinojima, and S. Itabashi, "Ultrasmall polarization splitter based on silicon wire waveguides," *Opt. Express*, vol. 14, no. 25, pp. 12401–12408, 2006.

[7] J. Wang, D. Liang, Y. Tang, D. Dai, and J. E. Bowers, "Realization of an ultra-short silicon polarization beam splitter with an asymmetrical bent directional coupler," *Opt. Lett.*, vol. 38, no. 1, pp. 4–6, 2013.

[8] F. Zhang, H. Yun, Y. Wang, Z. Lu, L. Chrostowski, and N. A. F. Jaeger, "Compact broadband polarization beam splitter using a symmetric directional coupler with sinusoidal bends," *Opt. Lett.*, vol. 42, no. 2, pp. 235–238, 2017.

[9] C. Li and D. Dai, "Compact polarization beam splitter based on a three-waveguide asymmetric coupler with a 340-nm-thick silicon core layer," *J. Lightw. Technol.*, vol. 36, no. 11, pp. 2129–2134, 2018.

[10] Y. Kim, M. H. Lee, Y. Kim, and K. H. Kim, "High-extinction-ratio directional-coupler-type polarization beam splitter with a bridged silicon wire waveguide," *Opt. Lett.*, vol. 43, no. 14, pp. 3241–3244, 2018.

[11] N. Zhao, C. Qiu, Y. He, Y. Zhang, and Y. Su, "Broadband polarization beam splitter by using cascaded tapered bent directional couplers," *IEEE Photon. J.*, vol. 11, no. 4, pp. 1–8, Jun. 2019.

[12] D. Dai, Z. Wang, and J. E. Bowers, "Ultrashort broadband polarization beam splitter based on an asymmetrical directional coupler," *Opt. Lett.*, vol. 36, no. 13, pp. 2590–2592, 2011.

[13] R. Halir *et al.*, "Waveguide sub-wavelength structures: A review of principles and applications," *Laser Photon. Rev.*, vol. 9, no. 1, pp. 25–49, 2015.

[14] V. Donzella, A. Sherwali, J. Flueckiger, S. T. Fard, S. M. Grist, and L. Chrostowski, "Sub-wavelength grating components for integrated optics applications on SOI chips," *Opt. Express*, vol. 22, no. 17, pp. 21037–21050, 2014.

[15] P. Cheben, R. Halir, J. H. Schmid, H. A. Atwater, and D. R. Smith, "Subwavelength integrated photonics," *Nature*, vol. 560, no. 7720, pp. 565–572, 2018.

[16] J. H. Schmid *et al.*, "Applications of subwavelength grating structures in silicon-on-insulator waveguides," in *Proc. SPIE*, vol. 7606, 2010, Art, no. 76060F.

[17] H. Xu, D. Dai, and Y. Shi, "Ultra-broadband and ultra-compact on-chip silicon polarization beam splitter by using hetero-anisotropic metamaterials," *Laser Photon. Rev.*, vol. 13, no. 4, 2019, Art. no. 1800349.

[18] C. Li, M. Zhang, J. E. Bowers, and D. Dai, "Ultra-broadband polarization beam splitter with silicon subwavelength-grating waveguides," *Opt. Lett.*, vol. 45, no. 8, pp. 2259–2262, 2020.

[19] K. Chen, K. Yu, and S. He, "High performance polarization beam splitter based on cascaded directional couplers assisted by effectively anisotropic structures," *IEEE Photon. J.*, vol. 11, no. 6, pp. 1–9, Dec. 2019.

[20] S. Jahani *et al.*, "Controlling evanescent waves using silicon photonic all-dielectric metamaterials for dense integration," *Nat. Commun.*, vol. 9, no. 1, 2018, Art. no. 1893.

[21] M. B. Mia, S. Z. Ahmed, I. Ahmed, Y. J. Lee, M. Qi, and S. Kim, "Exceptional coupling in photonic anisotropic metamaterials for extremely low waveguide crosstalk," *Optica*, vol. 7, no. 8, pp. 881–887, 2020.

[22] K. Jinguji, N. Takato, A. Sugita, and M. Kawachi, "Mach-Zehnder interferometer type optical waveguide coupler with wavelength-flattened coupling ratio," *Electron. Lett.*, vol. 26, no. 17, pp. 1326–1327, 1990.

[23] J. Van Campenhout, W. M. Green, S. Assefa, and Y. A. Vlasov, "Low-power, 2 x 2 silicon electro-optic switch with 110-nm bandwidth for broadband reconfigurable optical networks," *Opt. Express*, vol. 17, no. 26, pp. 24020–24029, 2009.

[24] T. Uematsu, T. Kitayama, Y. Ishizaka, and K. Saitoh, "Ultra-broadband silicon-wire polarization beam combiner/splitter based on a wavelength insensitive coupler with a point-symmetrical configuration," *IEEE Photon. J.*, vol. 6, no. 1, pp. 1–8, Feb. 2014.

[25] K. Jinguji, N. Takato, Y. Hida, T. Kitoh, and M. Kawachi, "Two-port optical wavelength circuits composed of cascaded Mach-Zehnder interferometers with point-symmetrical configurations," *J. Lightw. Technol.*, vol. 14, no. 10, pp. 2301–2310, 1996.

[26] F. Vogelbacher, S. Nevlacsil, M. Sagmeister, J. Kraft, K. Unterrainer, and R. Hainberger, "Analysis of silicon nitride partial euler waveguide bends," *Opt. Express*, vol. 27, no. 22, pp. 31394–31406. 2019.

[27] L. Zhang *et al.*, "Ultrahigh-Q silicon racetrack resonators," *Photon. Res.*, vol. 8, no. 5, pp. 684–689, 2020.

[28] Z. Xu, T. Lyu, and X. Sun, "Interleaved subwavelength gratings strip waveguide based TM pass polarizer on SOI platform," *IEEE Photon. J.*, vol. 12, no. 2, pp. 1–10, Apr. 2020.